

Molecular Beam Epitaxy of β -($\text{In}_x\text{Ga}_{1-x}$) $_2\text{O}_3$ on β - Ga_2O_3 (010): Compositional Control, Layer Quality, Anisotropic Strain Relaxation, and Prospects for Two-Dimensional Electron Gas Confinement

Piero Mazzolini,* Charlotte Wouters, Martin Albrecht, Andreas Falkenstein, Manfred Martin, Patrick Vogt, and Oliver Bierwagen

Cite This: <https://doi.org/10.1021/acsami.3c19095>

Read Online

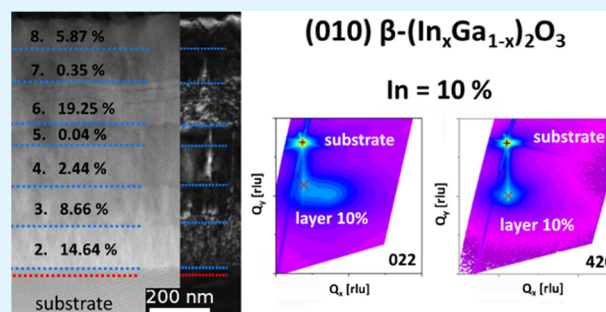
ACCESS |

Metrics & More

Article Recommendations

ABSTRACT: In this work, we investigate the growth of monoclinic β -($\text{In}_x\text{Ga}_{1-x}$) $_2\text{O}_3$ alloys on top of (010) β - Ga_2O_3 substrates via plasma-assisted molecular beam epitaxy. In particular, using different *in situ* (reflection high-energy electron diffraction) and *ex situ* (atomic force microscopy, X-ray diffraction, time-of-flight secondary ion mass spectrometry, and transmission electron microscopy) characterization techniques, we discuss (i) the growth parameters that allow for In incorporation and (ii) the obtainable structural quality of the deposited layers as a function of the alloy composition. In particular, we give experimental evidence of the possibility of coherently growing (010) β -($\text{In}_x\text{Ga}_{1-x}$) $_2\text{O}_3$ layers on β - Ga_2O_3 with good structural quality for x up to ≈ 0.1 . Moreover, we show that the monoclinic structure of the underlying (010) β - Ga_2O_3 substrate can be preserved in the β -($\text{In}_x\text{Ga}_{1-x}$) $_2\text{O}_3$ layers for wider concentrations of In ($x \leq 0.19$). Nonetheless, the formation of a large amount of structural defects, like unexpected (10 $\bar{2}$) oriented twin domains and partial segregation of In is suggested for $x > 0.1$. Strain relaxes anisotropically, maintaining an elastically strained unit cell along the a^* direction vs plastic relaxation along the c^* direction. This study provides important guidelines for the low-end side tunability of the energy bandgap of β - Ga_2O_3 -based alloys and provides an estimate of its potential in increasing the confined carrier concentration of two-dimensional electron gases in β -($\text{In}_x\text{Ga}_{1-x}$) $_2\text{O}_3$ / $(\text{Al}_y\text{Ga}_{1-y})_2\text{O}_3$ heterostructures.

KEYWORDS: β - Ga_2O_3 alloys, oxides semiconductor epitaxy, structural defects, compositional control, multilayer structure



1. INTRODUCTION

Gallium oxide has recently been earning large attention as a promising semiconductor for new-generation electronics. It has five different polymorphs,¹ and because of its intrinsic ultrawide bandgap, its future application is especially related, but not limited, to the fields of power electronics^{2,3} and solar-blind UV photodetectors.⁴ In particular, its thermodynamically stable crystal phase—monoclinic β - Ga_2O_3 —exhibits a bandgap of ≈ 4.7 eV,⁵ while its electronic conductivity can be controlled over a wide range throughout n-type extrinsic doping.² Differently from the other polymorphs, bulk β - Ga_2O_3 can be grown from the melt.^{6–8} This allows to (i) have bulk material from semi-insulating to conducting with low structural defectivity and (ii) employ it after substrate fabrication for the thin film deposition of homo- or hetero- Ga_2O_3 -based multilayer structures.

Similar to the AlGaIn-InGaN system, Ga_2O_3 can be alloyed with Al_2O_3 and In_2O_3 virtually allowing for bandgap engineering of the material between ≈ 3 eV (low-end side of bixbyite In_2O_3) and ≈ 9 eV (high-end side of corundum α - Al_2O_3).⁹

The bandgap control in Ga_2O_3 -based alloys enables charge carrier confinement at heterostructure interfaces, i.e., allowing the confinement of two-dimensional electron gases (2DEGs) that could help in the realization of high electron mobility transistors.¹⁰ In particular, a higher conduction band offset allows for the confinement of a higher sheet density of electrons in these 2DEGs. Nonetheless, the (In-Al-Ga) $_2\text{O}_3$ system has to account for different thermodynamically stable crystal structures of the binary end-members, setting up solubility limitations for the obtainable heterostructures. Due to the presence of bulk β - Ga_2O_3 substrates, the monoclinic crystal structure has been so far the only one capable of providing heterostructures with both low structural defectivity

Received: December 20, 2023

Revised: February 9, 2024

Accepted: February 18, 2024

and surface roughness suitable for the obtainment of 2DEGs.^{10–13}

In particular, 2DEG confinement has been experimentally demonstrated just at the β -(Al_yGa_{1-y})₂O₃/Ga₂O₃ interface of heterostructures deposited on (010)-oriented β -Ga₂O₃ substrates by both molecular beam epitaxy (MBE) and metal-organic vapor phase epitaxy (MOVPE) techniques.^{10–13} The β -Ga₂O₃ substrate orientation and offcut are fundamental factors for the deposition of Ga₂O₃ homo-^{14–20} or heterostructures^{10–13,21,22} with (i) low structural defectivity, (ii) smooth surfaces, and (iii) comparably high growth rates (in the case of MBE). So far, the (010) orientation has been the only one capable of meeting all these requirements, although also other orientations like offcut (100)^{17,18,20,23} and (001)^{17,24} have recently demonstrated similar potential. Particular effort has been put towards the realization of (010) heterostructures with larger band offsets by increasing the Al incorporation into β -(Al_yGa_{1-y})₂O₃ layers. So far, an Al concentration as high as $y = 0.26$ was reported for δ -doped β -(Al_yGa_{1-y})₂O₃/Ga₂O₃ heterostructures deposited via MOVPE on (010)-oriented substrates. This structure confined a total sheet electron concentration [2DEG + potential contribution from the δ -doped β -(Al_yGa_{1-y})₂O₃] of $6.4 \times 10^{12} \text{ cm}^{-2}$.¹³

On the other hand, the lower bandgap side of the β -Ga₂O₃ based alloys, i.e., β -(In_xGa_{1-x})₂O₃, has not been thoroughly examined so far. In particular, just few works reported on (201)-oriented β -(In_xGa_{1-x})₂O₃ layers grown on c-plane sapphire [Al₂O₃(0001)] substrates.^{25–28} The layer quality on this substrate/orientation is most likely not compatible with the obtainment of 2DEGs due to the presence of a large amount of structural defects and high surface roughness¹⁷ at least without considering the employment of proper substrate offcuts to suppress the formation of rotational domains.²⁹ To the best of our knowledge, very few experimental works^{22,30} reported on the structural quality and alloy composition obtainable for β -(In_xGa_{1-x})₂O₃ layers deposited on β -Ga₂O₃ substrates, and their investigation was limited to the (100) growth orientation. Based on the theoretical prediction that the conduction band minimum of β -(In_xGa_{1-x})₂O₃ is lower than that of β -Ga₂O₃,^{31–33} we believe that the realization of good quality β -(In_xGa_{1-x})₂O₃ layers could help to realize larger conduction band offsets in β -(In_xGa_{1-x})₂O₃/(Al_yGa_{1-y})₂O₃ heterostructures compared to the β -Ga₂O₃/(Al_yGa_{1-y})₂O₃ ones for the confinement of 2DEGs with higher sheet electron concentrations. Toward this goal, the present work aims at providing experimental evidence on (i) the deposition parameters that allow for In incorporation and (ii) the structural quality and phase purity as a function of x in β -(In_xGa_{1-x})₂O₃ thin films deposited on (010) β -Ga₂O₃ substrates via plasma-assisted MBE (PAMBE).

Maccioni et al.^{31,32} as well as Peelaers et al.³³ theoretically predict In to replace Ga in the octahedral sites of the monoclinic structure, therefore suggesting a solubility limit of $x = 0.5$ for the β -(In_xGa_{1-x})₂O₃ alloy. An energetically favorable phase mix (monoclinic + bixbyite) has been, however, predicted for In concentrations exceeding 10–20 cation %.^{31,32} Experimentally, single phase β -(In_xGa_{1-x})₂O₃ powders were synthesized via solid-state reactions for x up to 0.44.³⁴ Phase-pure monoclinic (201)-oriented thin films with x up to ≈ 0.1 were MOVPE-grown on top of Al₂O₃(0001) substrates,²⁵ while the pulsed laser deposition technique allowed to widen x up to ≈ 0.2 for layers deposited on the same substrate.^{26,35} Similarly, Oshima et al.²⁷ investigated the

growth of (201)-oriented β -(In_xGa_{1-x})₂O₃ thin films on Al₂O₃(0001) with PAMBE reporting monoclinic phase-pure layers for x up to ≈ 0.3 ; nonetheless, the crystallinity of the layers (evaluated from X-ray diffraction, XRD) was reported to worsen while increasing the amount of incorporated In. Just from the XRD 2θ - ω scan reported in ref 27, however, it is not possible to clarify if the crystal phase obtained from the MBE growth of the (In_xGa_{1-x})₂O₃ is indeed monoclinic or if the presence of In triggered the formation of the orthorhombic κ polymorph whose {001} diffraction peaks are found to be at similar positions with respect to the (201) monoclinic structure.^{36,37} This is because the presence of an additional In³⁸ or Sn³⁹ flux during the MBE growth of Ga₂O₃ layers has been found to (i) widen the growth window of Ga₂O₃ toward higher substrate temperatures and (ii) stabilize the κ polymorph for heteroepitaxial films on Al₂O₃(0001).

The underlying mechanism has been described as metal exchange catalysis (MEXCAT) or metal-oxide-catalyzed epitaxy (MOCATAXY) in which the catalyst element (Sn/In) or its suboxide (SnO, In₂O) is preferably oxidized on the growth surface and exchanged subsequently by Ga due to the stronger Ga–O than catalyst–O bonds, thus forming the Ga₂O₃ layer.^{24,38–41} This metal exchange leads to a segregation and/or desorption of the catalyst during the growth process, with the possibility to deposit α -,⁴² β -,^{14,17,20,24} and κ -Ga₂O₃ layers^{38,39,43} (depending on the used substrate) with just limited amounts of the catalyst being incorporated. Consequently, the incorporation of In for the formation of phase-pure β -(In_xGa_{1-x})₂O₃ alloys is particularly challenging in MBE. Vogt and Bierwagen²⁸ gave experimental guidelines for the MBE deposition of (In_xGa_{1-x})₂O₃ alloys on Al₂O₃(0001) substrates, pointing out that lower substrate temperatures and/or higher oxygen fluxes allow for the kinetically driven incorporation of larger amounts of In; nonetheless, in that work no details about the obtained crystal phase (i.e., β and/or κ) and quality of the deposited alloyed layers were given. Recently, Ardenghi et al.,⁴⁴ have experimentally shown that the stabilization of the β phase upon MEXCAT is mostly related to the overcome of the T -stability window of the metastable κ polymorph, i.e., for growth temperatures $T_g \geq 700 \text{ }^\circ\text{C}$ just monoclinic layers are synthesized despite the employment of the catalyst element and use of Al₂O₃(0001) substrate.

The present work starts from these experimental findings and aims at clarifying the possibility of depositing high crystal quality β -(In_xGa_{1-x})₂O₃ layers on β -Ga₂O₃ substrates by MEXCAT MBE/MOCATAXY with a focus on the (010) surface orientation. The reported results are discussed in view of its possible application in β -(In_xGa_{1-x})₂O₃/(Al_yGa_{1-y})₂O₃ heterostructures for the improved confinement of 2DEGs.

2. EXPERIMENTAL SECTION

In order to provide rapid, efficient, and economic screening of growth parameters, a multilayer sample (sample PM) consisting of seven different β -(In_xGa_{1-x})₂O₃ layers has been deposited on top of an Fe-doped (010)-oriented β -Ga₂O₃ substrate via PAMBE. Its growth sequence is schematically shown in Figure 1 and details on the experimental setup and substrate preparation are given in ref 14. Ga and In-fluxes were measured by an ion-gauge as beam equivalent pressure (BEP) and converted into particle flux ($\text{nm}^{-2} \text{ s}^{-1}$) by measuring the respective oxide growth rate under conditions of full cation incorporation as described in refs.14,21,40 The Ga-flux, plasma power, and deposition time for the β -(In_xGa_{1-x})₂O₃ layers in PM were fixed at $\Phi_{\text{Ga}} = 2.34 \text{ nm}^{-2} \text{ s}^{-1}$, 300 W, and $t = 30 \text{ min}$, respectively. For the investigation of the effect of deposition

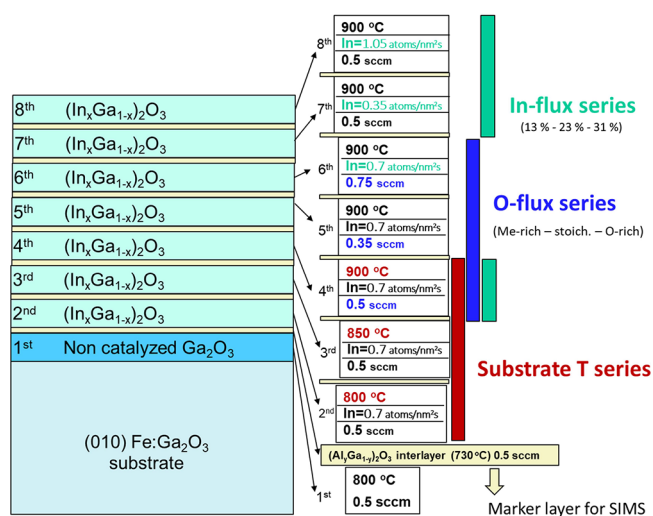


Figure 1. Exemplary drawing of the experimental design for the multilayer structure and of the investigated growth parameters (fixed Ga-flux of $2.34 \text{ Ga nm}^{-2} \text{ s}^{-1}$, plasma power of 300 W and varied substrate temperature, O-flux, and In-flux as indicated).

parameters, we varied the O-flow (0.35, 0.5, 0.75 standard cubic centimeter per minute [sccm]), substrate temperature ($T_g = 800, 850, 900 \text{ }^\circ\text{C}$), and In-flux [$\Phi_{\text{In}} = 0.35, 0.7, \text{ and } 1.05 \text{ atoms}/(\text{nm}^2 \text{ s})$], corresponding to a nominal In concentration $x_{\text{nom}} = \Phi_{\text{In}} / (\Phi_{\text{Ga}} + \Phi_{\text{In}})$

$\Phi_{\text{Ga}} = 0.13, 0.23, 0.31$] indicated by red, blue, and light green bars, respectively, in Figure 1. $\beta\text{-(Al}_y\text{Ga}_{1-y})_2\text{O}_3$ tracing/marker layers, indicated by yellow horizontal bars in Figure 1, were deposited between the $\beta\text{-(In}_x\text{Ga}_{1-x})_2\text{O}_3$ to facilitate secondary ion mass spectrometry (SIMS) investigation. These layers were deposited for $t = 80 \text{ s}$ at $T_g = 730 \text{ }^\circ\text{C}$, Al cell $T = 1008 \text{ }^\circ\text{C}$, and O-flow = 0.5 sccm, resulting in a nominal thickness of 2–5 nm and expected Al content of $y \approx 0.05$ that is not expected to affect the structural quality of the stack.¹⁷

The multilayer sample was monitored *in situ* by reflection high-energy electron diffraction (RHEED) to assess the layer quality.

In addition, single $(\text{In}_x\text{Ga}_{1-x})_2\text{O}_3$ layer samples (P02, P10, U09, U13, and U19) with In content between 2 and 19 cation % were deposited as summarized in Table 1. These single layers were deposited in two different PAMBE chambers indicated by the sample names starting with P (Paul Drude Institute) and U (University of California at Santa Barbara), with PDI also being the one in which the multilayer structure was deposited (PM). Both chambers are equipped with an apparatus similar to the one previously described. The oxygen plasma units of the two MBE apparatuses were SPECS PCS and VEECO Unibulb whose O-flow rates were controlled by mass-flow controllers and foreline pressure controllers for P and U, respectively. Further details for the growth chamber of samples U09–U19 can be found in ref 21.

The surface morphology of all samples was scanned with atomic force microscopy (AFM; Bruker Dimension Edge) in the PeakForce tapping mode. Their In-content was determined with time-of-flight ToF-SIMS using ToF-SIMS IV from IONTOF GmbH. The quantitative ToF-SIMS calibration of the In concentration was

Table 1. Overview of the Investigated $\beta\text{-(In}_x\text{Ga}_{1-x})_2\text{O}_3$ Layers^a

sample	GR [nm/min]	In content (SIMS) [%]	thickness [nm]	b [Å]	T_g [$^\circ\text{C}$]	Ga BEP/flux Φ_{Ga} [10^{-7} mbar/nm ² s ⁻¹]	In BEP/flux Φ_{In} [10^{-7} mbar/nm ² s ⁻¹]	$x_{\text{nom}} = \Phi_{\text{In}} / (\Phi_{\text{Ga}} + \Phi_{\text{In}})$	oxygen flow/foreline pressure/plasma power [sccm/Torr/W]
$\beta\text{-Ga}_2\text{O}_3$ substrate		0		3.040					
PM		0–19, see Figure 2	...		see Figure 1	1.9/2.34	see Figure 1		see Figure 1
PM_2	4.3 ± 0.2	14.64 ± 0.3	130 ± 6		800	1.9/2.34	1.3/0.7	0.23	0.5/–/300
PM_3	3.7 ± 0.2	8.66 ± 0.2	112 ± 5		850	1.9/2.34	1.3/0.7	0.23	0.5/–/300
PM_4	3.6 ± 0.2	2.44 ± 0.04	108 ± 5		900	1.9/2.34	1.3/0.7	0.23	0.5/–/300
PM_5	1.9 ± 0.1	0.04 ± 0.004	58 ± 4		900	1.9/2.34	1.3/0.7	0.23	0.35/–/300
PM_6	4.1 ± 0.2	19.25 ± 0.2	124 ± 5	...	900	1.9/2.34	1.3/0.7	0.23	0.75/–/300
PM_7	2.9 ± 0.2	0.35 ± 0.04	88 ± 5		900	1.9/2.34	0.65/0.35	0.13	0.5/–/300
PM_8	3.5 ± 0.1	5.87 ± 0.2	106 ± 4		900	1.9/2.34	1.95/1.05	0.31	0.5/–/300
P02	3.5 ± 0.1	2.48 ± 0.3	105 ± 2	3.047	800	1.9/2.34	1.3/0.7	0.23	0.33/–/300
P10	4.1 ± 0.1	10.05 ± 0.3	122 ± 2	3.082	850	1.9/2.34	1.3/0.7	0.23	0.5/–/300
U09	3.9 ± 0.1	9.12 ± 0.3	164 ± 3	3.069	950	1.1/2	2.3/2.5	0.56	–/60/200
U13	3.9 ± 0.1	13.04 ± 0.3	177 ± 4	3.084	900	1.1/2	1/1.1	0.35	–/60/200
U19	4.4 ± 0.1	19.48 ± 1.3	155 ± 3	3.10	900	1.1/2	1/1.1	0.35	–/80/200

^aDetermined growth rate (GR), In content, layer thickness, and out-of-plane lattice parameter b determined by HRXRD of the 020 reflex, as well as growth parameters (Ga- and In-beam equivalent pressures [BEP] and corresponding fluxes, oxygen flow rate or foreline pressure, and plasma power) are given. For the single layers, the number following the initial letter reflects the In amount rounded to integer cation % in the $\beta\text{-(In}_x\text{Ga}_{1-x})_2\text{O}_3$ corresponding alloy. The In content determined by SIMS is the mean value in the plateaus regions of the analyzed layers; the corresponding uncertainties are related to the standard deviations. For the thickness of the layers (SIMS), the error has been set to 2% (crater depth from interference microscopy Veeco Instruments, Inc.); in the case of the PM multilayer, the error over the determined thickness has been also compensated according to the uncertainty level over the thickness of the $\beta\text{-(Al}_y\text{Ga}_{1-y})_2\text{O}_3$ tracing/marker layers.

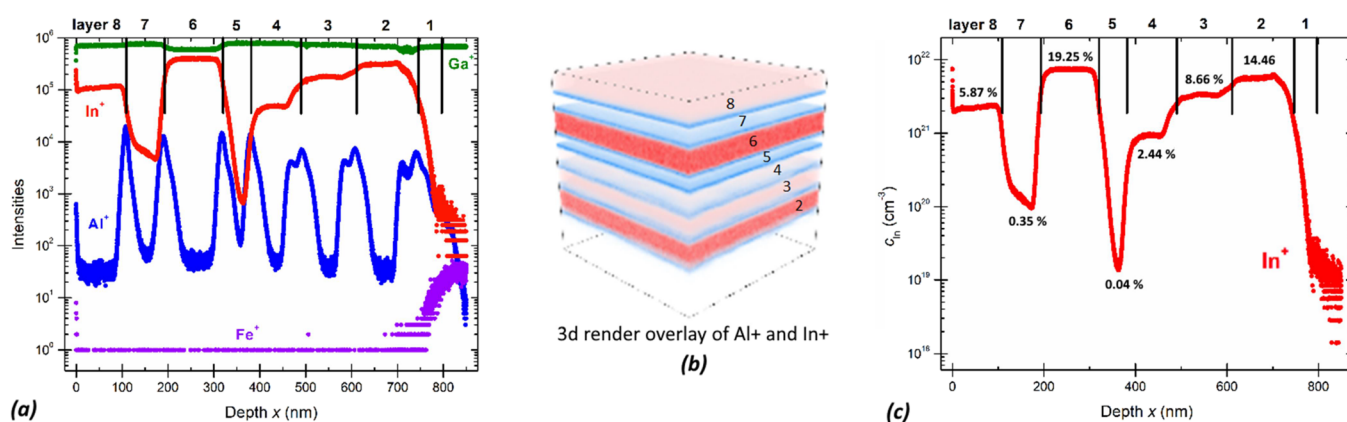


Figure 2. ToF-SIMS of the multilayer sample PM: (a) depth profile of Ga, In, Al, and Fe secondary ions, (b) 3d render overlay of a $100 \times 100 \mu\text{m}$ area indicating In (red) and Al (blue) secondary ions, and (c) calibrated In concentration profile.

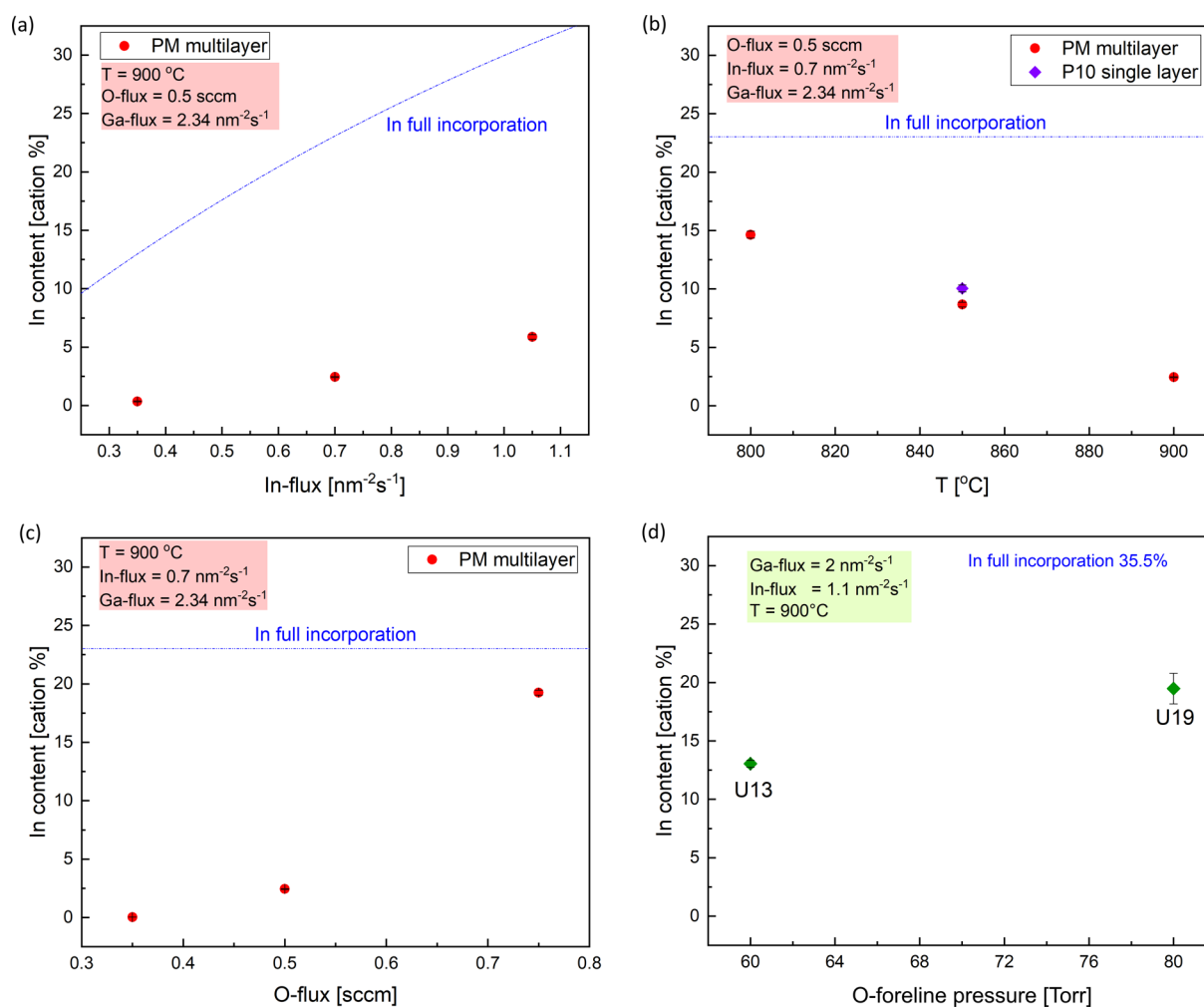


Figure 3. Dependence of In content on to the provided (a) In-flux, (b) substrate T , and (c) O_2 -flux (plasma $P = 300 \text{ W}$)/(d) O_2 -foreline pressure (plasma $P = 200 \text{ W}$) for the $\beta\text{-(In}_x\text{Ga}_{1-x})_2\text{O}_3$ multilayer (PM disks) and single layers (squares, violet PDI and green UCSB). The full set of data is reported in Table 1.

obtained from pulsed laser deposited $(\text{In}_x\text{Ga}_{1-x})_2\text{O}_3$ reference films on $\text{Al}_2\text{O}_3(0001)$ substrates analyzed by energy-dispersive X-ray analysis as explained in detail in ref 17. XRD measurements (PANalytical X'Pert Pro MRD using $\text{Cu K}\alpha$ radiation) were performed on all samples. Symmetric, out-of-plane 2θ - ω scans and ω -rocking curves of the 020 reflex along the c^* (001) and a^* (100) in-plane directions as well as reciprocal space maps of the 420 and 022

reflexes were performed to investigate the out-of-plane lattice parameter as well as the strain relaxation of the layers, respectively. The out-of-plane lattice parameters were additionally measured by high-resolution XRD (HRXRD). Cross-sectional transmission electron microscopy (TEM—aberration-corrected FEI Titan 80–300 operating at 300 kV) along the [001] direction was carried out on the multilayer sample. Scanning TEM (STEM) images were recorded

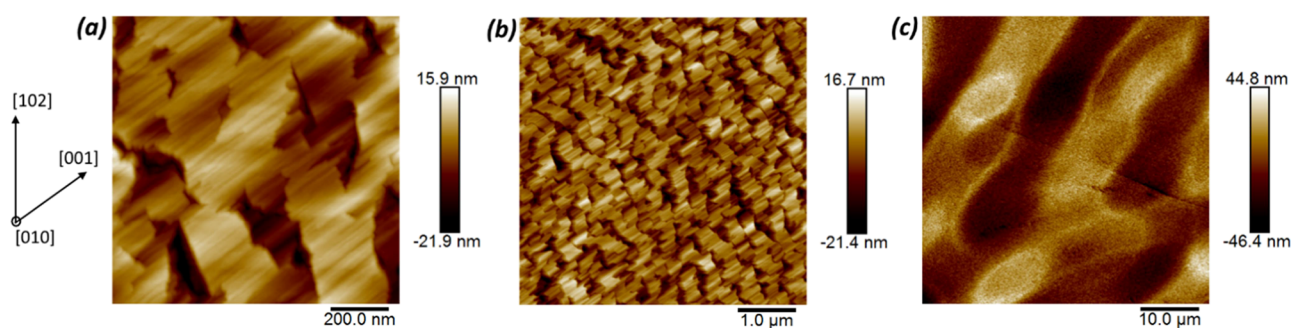


Figure 4. AFM topographs of the multilayer for 1×1 , 5×5 , and $50 \times 50 \mu\text{m}^2$ scanned areas for (a), (b), and (c), respectively. Height scale and in-plane direction are indicated.

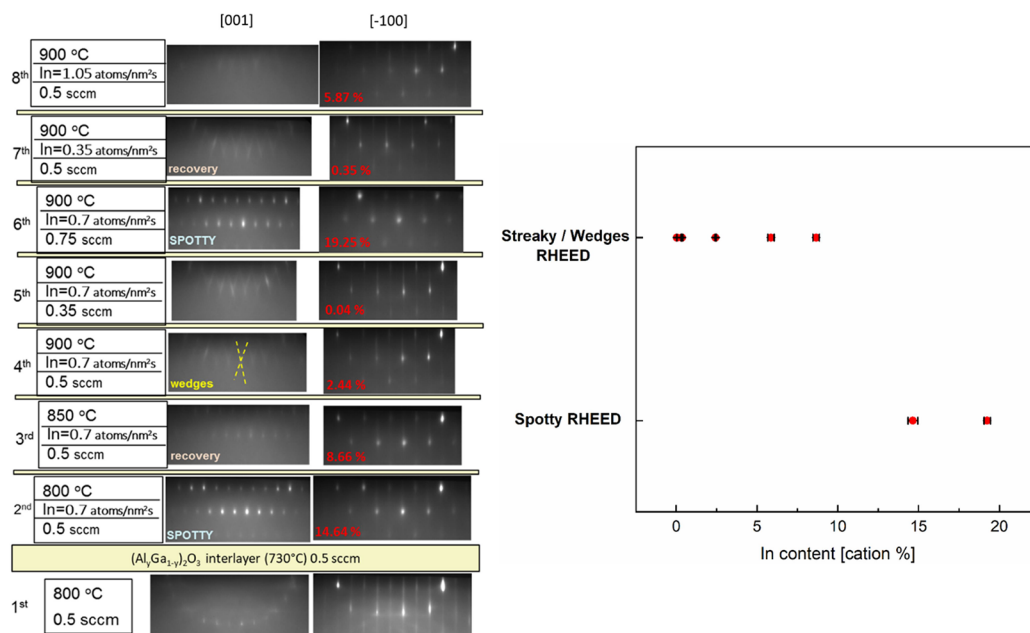


Figure 5. RHEED images from [001] and $[-100]$ azimuths taken in situ after the deposition of every single β -(In_xGa_{1-x})₂O₃ layer of sample PM; a qualitative dependence of the RHEED pattern with respect to the In incorporation is also provided.

with a high-angle annular dark-field (HAADF) detector with an inner acceptance angle of 35 mrad and a camera length of 196 mm.

3. RESULTS AND DISCUSSION

3.1. Indium Incorporation. The multielemental intensity signals collected via ToF-SIMS in depth profiling for the multilayer (Figure 2a) allow us to distinguish all the eight deposited layers (sample PM). Apart from the different In⁺ signal collected for the individual layers, the presence of the β -(Al_xGa_{1-x})₂O₃ markers helps to better define the respective thicknesses (Figure 2a,b). The presence of a wider Al⁺ intensity distribution for deeper probing depths should be ascribed to the roughening of the layer throughout the sputtering process (Figure 2a).

The In concentrations (evaluated as cationic %) obtained in the multilayer structure span from a minimum of 0.04 to a maximum of 19.25%. Using these SIMS results, under the hypothesis that all of the detected In is present as Ga substitutional (i.e., In_{Ga}), we report in Figure 3a–c (red circles) the In incorporation dependence with the main three tested synthesis parameters (see Figure 1) during the multilayer deposition. In Figure 3a, we identify a monotonic increase in In with increasing In-flux (fixed $T_g = 900$ °C and

0.5 sccm). Nonetheless, under such fixed growth conditions, the maximum In incorporation was limited to 5.87% (i.e., low incorporation efficiency). The substrate temperature plays an important role in the In-flux incorporation (fixed O-flux = 0.5 sccm and In-flux = $0.7 \text{ nm}^{-2} \text{ s}^{-1}$, Figure 3b), showing an almost monotonic decrease while increasing T from 800 to 900 °C (maximum In concentration of 14.64%); on the same graph, the data referred to the single-layer P10 (violet square) is demonstrating the reproducibility of the collected experimental data and at the same time excluding any major effects related to the multilayer approach (e.g., effect from underlying layers). A superlinear increase (Figure 3c) in the In incorporation is recorded while increasing the O-flux (fixed $T_g = 900$ °C and In-flux = $0.7 \text{ nm}^{-2} \text{ s}^{-1}$): in this case, despite the high T_g , a maximum In incorporation of about 19.25% is obtained. In this case, the data collected on single layers deposited in a different PAMBE apparatus qualitatively confirm the dependence of In incorporation on the provided oxygen flux (Figure 3d). More in general, even if two different MBE experimental apparatus and various deposition parameters were employed, a comparison among all of the single layers reported in Table 1 (i.e., P02, P10, U09, U13, U19), allows to qualitatively confirm that the provided oxygen and

the substrate temperature are the major growth parameters affecting the In incorporation in the $(\text{In}_x\text{Ga}_{1-x})_2\text{O}_3$ alloy. These recorded dependencies of the synthesis parameters with respect to the In-flux incorporation are qualitatively similar to what has been previously observed during plasma-assisted MBE of κ -, β -, as well as α - $(\text{In}_x\text{Ga}_{1-x})_2\text{O}_3$ alloys [*c*-plane sapphire substrates with and without β - $\text{Ga}_2\text{O}_3(-201)$ nucleation layers for κ and β , *m*-plane sapphire substrate for α].^{28,44–46}

3.2. Impact of In Content x on Structural Quality.

3.2.1. Surface Morphology. AFM on 1×1 and $5 \times 5 \mu\text{m}^2$ area scans of the multilayer PM sample (Figure 4a,b) shows features already highlighted for other (010) homoepitaxial β - Ga_2O_3 layers, i.e., (110) and $(\bar{1}10)$ facets visible as elongated features along [001] and deeper trenches almost orthogonal to them.^{14,19} The image with the largest scan area of $50 \times 50 \mu\text{m}^2$ (Figure 4c) shows that some inhomogeneity is present in the multilayer. This is most likely related to the different growth conditions that were already shown to affect the quality of the deposited layers in the case of (010) β - Ga_2O_3 homoepitaxy.¹⁴

In Figure 5, the RHEED images taken *in situ* after the deposition of the individual layers of sample PM are reported. It is possible to identify a better quality of the RHEED images for an In content up to 8.66% (i.e., passage from wedges and streaks for the [001] and $[-100]$ azimuths, respectively, to a spotty pattern). The presence of wedges in the RHEED images acquired along the [001] azimuth is related to the (110)-faceting¹⁴ of the (010)-oriented β - $(\text{In}_x\text{Ga}_{1-x})_2\text{O}_3$ layers. The presence of these shallow facets is independently confirmed by the AFM images acquired for the single-layer samples (Figure 6). For $x \geq 0.13$, the AFM single-layer morphology lacks

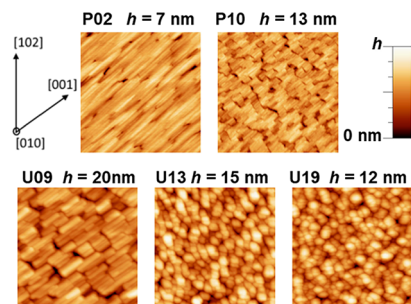


Figure 6. $1 \times 1 \mu\text{m}$ AFM images of the β - $(\text{In}_x\text{Ga}_{1-x})_2\text{O}_3$ single layers (details in Table 1).

oriented features and exhibits a grainy morphology. Nonetheless, we stress that it could be misleading to attribute the discussed morphology transition just to the content of In: both x and other growth parameters (e.g., T_g , metal-to-oxygen flux ratio) can compete in determining the observed AFM morphologies.

3.2.2. Phase Stability and Microstructure. All samples were investigated via XRD. The wide-range symmetric out-of-plane 2θ - ω scans of the multilayer sample PM and the single layers U09–U19, reported in Figure 7, show strong reflexes in the vicinity of the 020 β - Ga_2O_3 main substrate reflection, which are related to the β - $(\text{In}_x\text{Ga}_{1-x})_2\text{O}_3$ layers and β - $(\text{Al}_y\text{Ga}_{1-y})_2\text{O}_3$ marker layers. The absence of additional strong reflexes in the XRD of the PM multilayer suggests that all layers maintain a single monoclinic phase despite the wide range of In incorporation (as later confirmed by TEM). Therefore, differently from the growth on (100) β - Ga_2O_3 substrates,²²

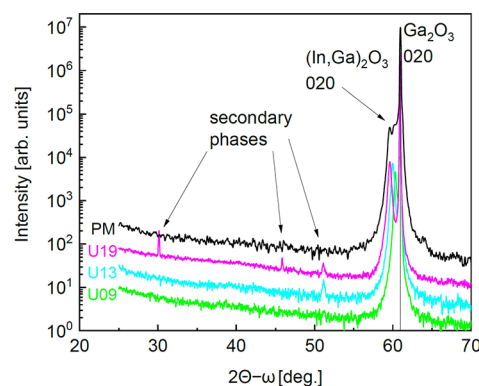


Figure 7. Exemplary wide-range XRD 2θ - ω scans are used to identify secondary phases.

the MBE growth on the (010) orientation allows for In incorporation of at least as high as $\approx 19\%$ for pure β - $(\text{In}_x\text{Ga}_{1-x})_2\text{O}_3$ alloyed layers. Only for U13 and U19, weak additional reflexes can be observed, suggesting the possible formation of a minor fraction of secondary orientations or secondary phases for an In-content exceeding 10%. These secondary phases/orientations may cause the grainy morphology visible in the AFM images of these single layers (Figure 6). The appearance of possible secondary phases in the U single layers has not been further investigated; nevertheless, our results collected from two different MBE systems suggest that slightly different synthesis parameters could eventually result in small fractions of different phases from the pure monoclinic one for $x > 0.1$.

The impact of In incorporation on the layer microstructure is analyzed in detail by means of TEM for each layer of the PM multilayer. For this purpose, the cross-sectional structure is viewed in the [001] projection. HAADF STEM and weak beam dark-field (WBDF) TEM overview images are presented in Figure 8a,b. In the HAADF image, the intensity is qualitatively proportional to the mean atomic number of the material. This allows us to distinguish the single layers with different compositions based on intensity, and the highest indium content layers estimated from SIMS (second and sixth) indeed appear the brightest. The contrast in each layer is not homogeneous though, and additional intensity effects can be caused by composition fluctuations, lattice defects, or differences in strain or orientation. The interface between subsequent layers starts out rather smooth but gets rougher as the number of deposited layers increases. The resulting surface also is rough with peak-to-valley distances on the order of a few nanometers but without the formation of clear facets with defined angles, as observed in the MBE growth of (010) β - Ga_2O_3 .¹⁴ In the 19.25% layer, two horizontal dark intensity bands of ~ 10 nm thickness can be observed. Higher magnification images of those regions showed no disruption of the monoclinic structure; therefore, it is not caused by phase separation. We rather suspect there was some unintentional change in growth parameter (e.g., fluctuation of plasma power) during deposition, which resulted temporarily in a lower indium content. The WBDF image on the right is produced by selecting only one diffraction spot and tilting the sample slightly off Bragg condition, which basically means defects will “light up” in the image. The brightest intensity in the highest indium-containing layers indicates the highest formation of defects there, i.e., lowering of the crystalline quality. The

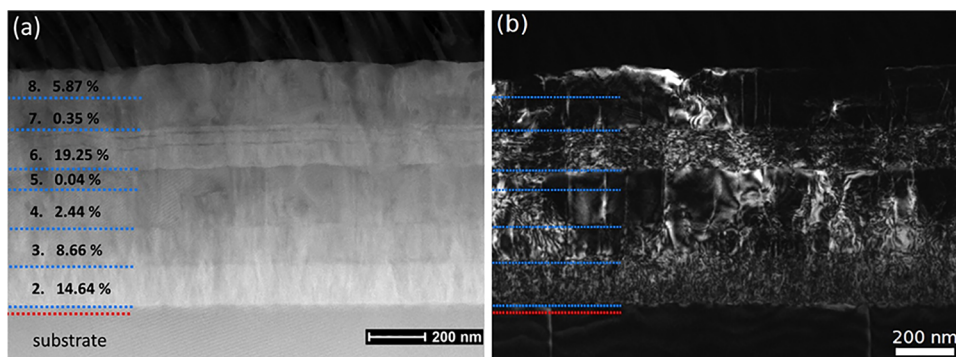


Figure 8. (a) HAADF STEM and (b) dark-field TEM overview images of the complete structure of sample PM, imaged in cross-section in the [001] projection of the Ga_2O_3 substrate.

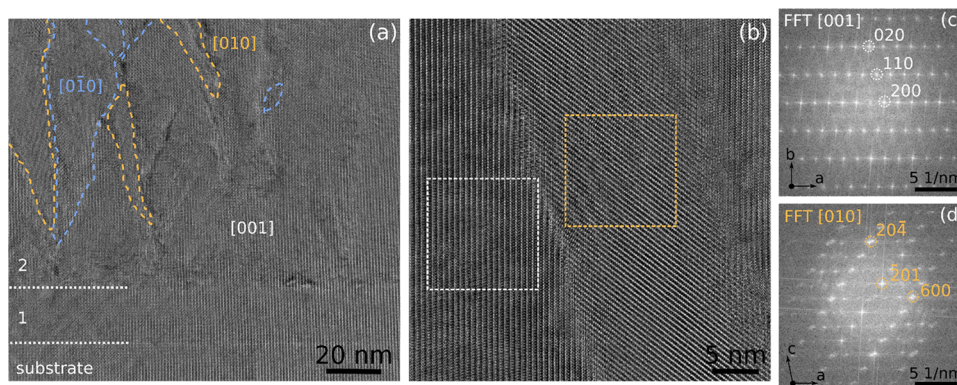


Figure 9. (a) HRTEM image of sample PM showing the formation of $[010]$ and $[0\bar{1}0]$ projected twinned grains in the 2nd layer with 14.64% In. (b) Higher magnification image of a $[010]$ -projected grain (orange) embedded in the $[001]$ -projected matrix (white), within (c) and (d) the FFTs of both areas.

defects are often transferred into the overgrown layers, but an overall decrease in WBDF intensity with a lowering of the indium content shows a “recovery” in the crystal structure, consistent with the recovery observed in situ by RHEED. High-resolution TEM (HRTEM) in the high indium-containing parts of the PM multilayer structure (i.e., 14.64 and 19.25% In layers) was performed to investigate more deeply what is causing the extended defects formation. As illustrated in Figure 9a,b for the 14.4% In layer, grains with an HRTEM pattern differing from the expected $[001]$ projected $[(010)$ -oriented] structure are observed. From the fast Fourier transform (FFT) of such a grain, it is found that they correspond to a different projection of the monoclinic phase, namely, $[010]$ projection with growth along $(20\bar{4})$, as illustrated in Figure 9d. Domains of both twin orientations $[010]$ and $[0\bar{1}0]$, colored in light orange and blue, respectively, in Figure 9a, are found. They start to form in the second layer with 14.64% In and again in the sixth layer with 19.25% In and some penetrate through to the next layer or even further. However, on average they are disappearing as the structure gets overgrown with material of lower indium content. The twin domains appear slightly brighter in the HAADF STEM image, which seems to indicate that indium is segregating in those grains. This could explain the deviation of the out-of-plane lattice parameter to lower values for indium content $>14\%$ (Figure 11) since these are based only on (010) -oriented material.

Thus, despite maintaining the monoclinic structure for all investigated compositions, indium can be incorporated at least

up to approximately 10% as a single-orientation/phase layer with low structural defectivity and without indium segregation.

3.3. Lattice Parameters and Anisotropic In-Plane Strain Relaxation. 3.3.1. Out-of-Plane Lattice Parameter b .

Figure 10 shows detailed 2θ - ω scans in the vicinity of the

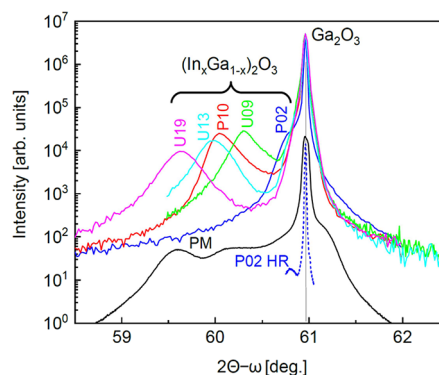


Figure 10. XRD 2θ - ω scans of the layer reflexes of all samples in the vicinity of the 020 β - Ga_2O_3 reflex.

020 substrate reflex for all of the samples. For PM, the convolution of several reflexes at the left side of the substrate reflex is related to the β - $(\text{In}_x\text{Ga}_{1-x})_2\text{O}_3$ layers with different compositions and lattice parameter b larger than that of pure β - Ga_2O_3 . Only the position of the reflex at the lowest 2θ angle (layer with largest b , thus highest In content x) can be clearly determined. The single shoulder on the right-hand side of the

substrate reflex should be assigned to the seven β - $(\text{Al}_y\text{Ga}_{1-y})_2\text{O}_3$ marker layers (see Figures 1 and 2b), having a smaller b . With increasing In content, the corresponding XRD scans of the individually grown β - $(\text{In}_x\text{Ga}_{1-x})_2\text{O}_3$ single-layer samples exhibit, besides the substrate reflex, an additional broad reflex each at increasingly smaller 2θ angle, corresponding to increasingly larger b . To resolve the reflex position (shoulder) of the lowest In content sample, P02, we additionally show HRXRD.

Figure 11 shows the out-of-plane lattice parameter b of all β - $(\text{In}_x\text{Ga}_{1-x})_2\text{O}_3$ layers (measured by HRXRD) as a function of

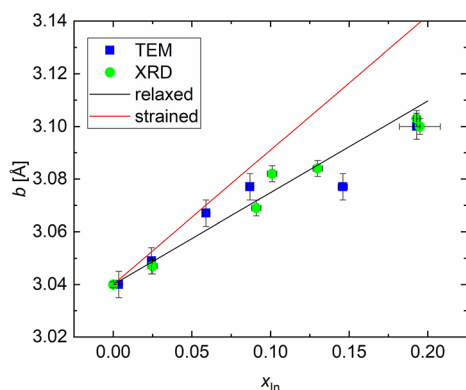


Figure 11. Lattice parameter b as a function of In content locally measured in sample PM by TEM diffraction patterns, as well as by XRD in the single layers. Black and red lines represent two extremes of fully relaxed and pseudomorphically strained β - $(\text{In}_x\text{Ga}_{1-x})_2\text{O}_3$ -layers using the relaxed lattice parameters published by Kranert et al.²⁶ for β - $(\text{In}_x\text{Ga}_{1-x})_2\text{O}_3$ powders and calculations of biaxially strained (010) layers from Oshima et al.,⁴⁷ respectively. $b = 3.040$ Å was assumed consistently for β - Ga_2O_3 in line with our HRXRD measurements of the substrate 020 reflection.

In-content. For sample PM, b was locally measured in all individual β - $(\text{In}_x\text{Ga}_{1-x})_2\text{O}_3$ layers by TEM-based selected area electron diffraction (SAED), placing a moveable aperture in the beamline such that only intensity from a specific β - $(\text{In}_x\text{Ga}_{1-x})_2\text{O}_3$ is contributing to the diffraction image. For all single layers and the highest-In-containing layer of PM, b was extracted from the β - $(\text{In}_x\text{Ga}_{1-x})_2\text{O}_3$ 020 reflex positions of XRD analysis (Figure 10). For reference, lines representing predicted values (based on literature as indicated) for fully relaxed or pseudomorphically strained films are also shown. The out-of-plane lattice parameters extracted by both methods show remarkable agreement and are approximately following the Vegard's law. For layers with In content below 10% inside sample PM, b could be well represented by the pseudomorphically strained scenario, whereas the relaxed scenario seems to better apply for larger In content (further discussion on this aspect based on reciprocal space maps of single layers, see Figure 12).

3.3.2. Coherent Growth and Anisotropic In-Plane Strain Relaxation. The larger lattice parameter of the β - $(\text{In}_x\text{Ga}_{1-x})_2\text{O}_3$ layer compared to that of the β - Ga_2O_3 substrate is prone to result in a compressive strain of the layer. To shed light on the strain state of the layer, the single-layer samples were further investigated by XRD reciprocal space maps. Figure 12 shows reciprocal space maps for the 022 and 420 reflexes of the samples P10, U09–U19, corresponding to c^* and a^* in-plane directions, respectively, to resolve potential anisotropies.

The positions of the substrate and layer reflexes are marked in Figure 12 and compiled in a systematic summary, shown in Figure 13, of strain relaxation for all single-layer samples. In this representation, the relative change of reciprocal space coordinates of the 020 (only vertical component), 022, and 420 reflexes with respect to those of the substrate is given for the out-of-plane (b) direction as well as in-plane directions (a^* and c^*), and the substrate reflex is at the origin (0, 0). Reference lines are drawn for pseudomorphically strained (vertical green dotted line) and fully relaxed scenarios (oblique solid lines). Due to different relative changes of a and c lattice parameters with increasing In content, two different lines are drawn, the black for the a^* in-plane component and the red one for the c^* . The star-shaped symbols indicate the expected values for relaxed β - $(\text{In}_{0.1}\text{Ga}_{0.9})_2\text{O}_3$.²⁶

For each sample, the vertical components extracted from all three reflexes are in good (within $\pm 0.1\%$) agreement and decrease with increasing In content, confirming a consistent set of data. The largest part of sample P10 with an In-content of 10% and 120 nm film thickness is coherently grown, indicated by coincidence of in-plane components in both directions (c^* and a^*) with those of the substrate (follow the green dotted line). This pseudomorphically strained scenario with compressive layer strain can also explain the increased out-of-plane lattice parameter b (due to the Poisson effect) that can be observed in the analysis of the 020 reflex (cf. Figures 10 and 11). Sample U09 with similar In content but a larger film thickness of 160 nm seems to exceed the critical thickness for strain relaxation as it shows some degree of relaxation and broader reflexes. For higher In content of about 13 and 19%, (almost complete) relaxation occurs only into the in-plane c^* direction (022 reflexes agree approximately with the red reference line), whereas the layer remains almost pseudomorphically strained in the a^* direction with partial relaxation for the 19% sample. The mosaic tilt, quantified by the full widths at half-maximum of the 020 ω -rocking curve, of the β - $(\text{In}_x\text{Ga}_{1-x})_2\text{O}_3$ layers along both the c^* and a^* in-plane directions is shown in Figure 14 as a function of In content. It monotonically increases with increasing In content and shows consistently larger values along the c^* than a^* direction, consistent with the plastic relaxation occurring just for $x > 0.1$ at first along the c^* direction.

The anisotropic in-plane strain relaxation found here, is similar to that observed for compressively strained α - $(\text{Al}_x\text{Ga}_{1-x})_2\text{O}_3$ films on a -plane α - Al_2O_3 substrates exhibiting fast in-plane plastic relaxation into the [001] via dislocation glide on the r -plane slip system and almost pseudomorphic strain in the $[-110]$ direction.^{48,49} The origin of the anisotropic strain relaxation in the (010)-oriented β - $(\text{In}_x\text{Ga}_{1-x})_2\text{O}_3$ layers investigated in this work remains to be explored. We speculate, that an easier compression of the a -direction compared to that of the c -direction⁵⁰ may facilitate the elastic strain in the a^* direction. Practical consequences of the anisotropic strain relaxation are (i) conclusions on pseudomorphically strained layers should be drawn based on investigation of the relaxation in the c^* rather than the a^* direction, and (ii) misfit dislocations formed during plastic strain relaxation into the c^* direction correspond to directional extended defects that will likely turn the fairly isotropic electrical conductivity,⁵¹ into one with anisotropic in-plane conductivity. For lateral field-effect transistors based on a β - $(\text{In}_x\text{Ga}_{1-x})_2\text{O}_3$ channel, this would result in reduced channel mobility along the c^* direction.

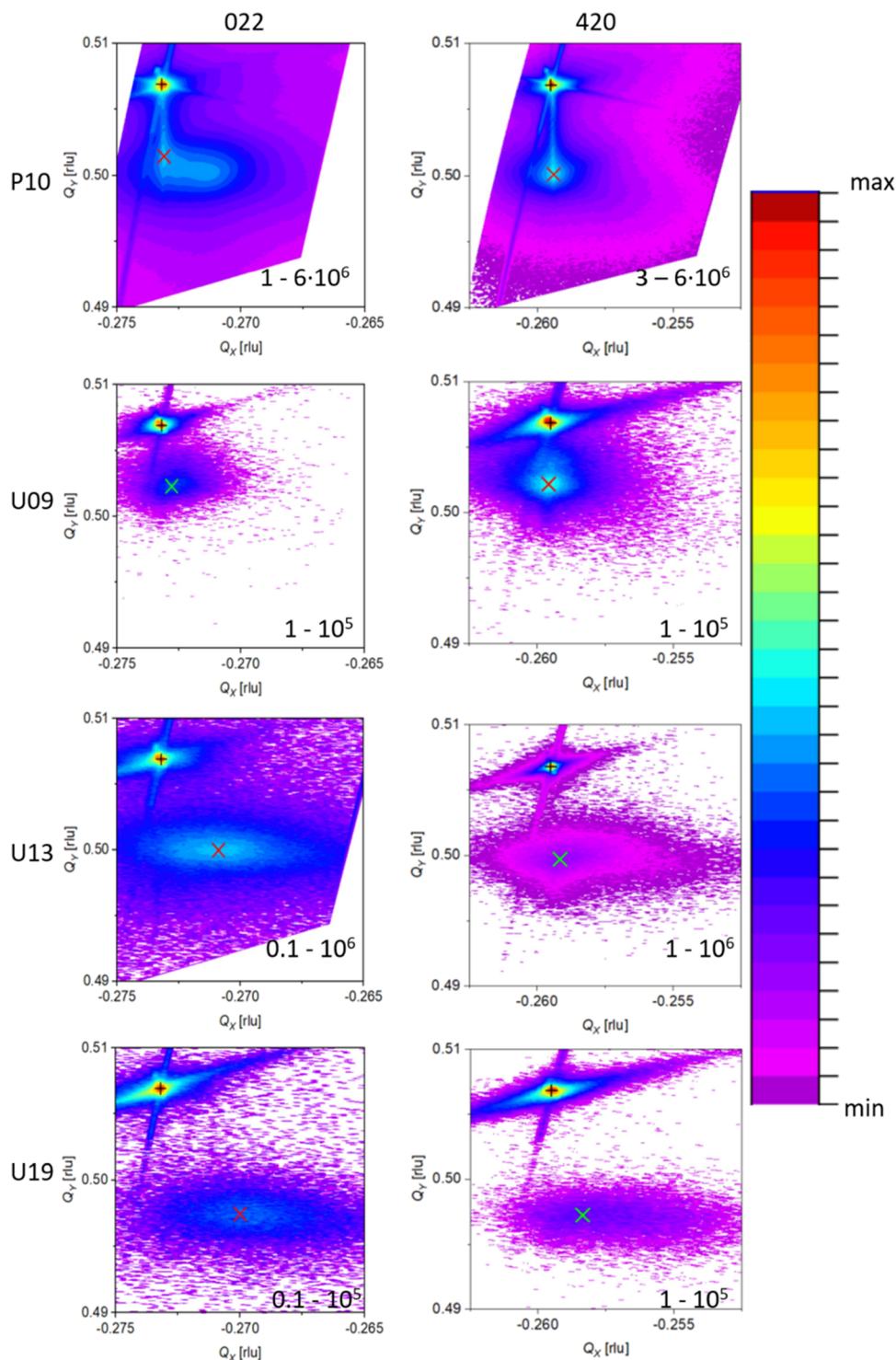


Figure 12. XRD reciprocal space maps of samples P10, U09, U13, and U19 taken for the 022 and 420 reflexes. The position of the sharp substrate reflex is marked by a “+,” whereas the broad reflex of the layer is marked by a “x”. The correspondence of the logarithmic color scale on the right side to minimum and maximum intensity is given in the maps.

3.4. Prospect of Two-Dimensional Electron Gases in a $(\text{In}_x\text{Ga}_{1-x})_2\text{O}_3/(\text{Al}_y\text{Ga}_{1-y})_2\text{O}_3$ Heterostructures. A potential application of β - $(\text{In}_x\text{Ga}_{1-x})_2\text{O}_3$ layers is the replacement of the β - Ga_2O_3 channel in a modulation-doped β - $(\text{Al}_y\text{Ga}_{1-y})_2\text{O}_3/\beta$ - Ga_2O_3 heterostructure to increase the confined sheet electron concentration n_s . In such heterostructures, n_s is mainly limited by its approximately linear dependence on the conduction band offset $\Delta E_C[\text{channel, barrier}]$ between the channel and

barrier material.⁵² The Al content in the barrier material, which determines $\Delta E_C[\beta\text{-Ga}_2\text{O}_3, \beta\text{-}(\text{Al}_y\text{Ga}_{1-y})_2\text{O}_3]$, is limited by phase separation. For example, a 2DEG with $n_s = 4.7 \times 10^{12} \text{ cm}^{-2}$ has been demonstrated for an Al content of $y = 0.17$ in the β - $(\text{Al}_y\text{Ga}_{1-y})_2\text{O}_3$ barrier material, corresponding to an estimated $\Delta E_C \approx 0.4 \text{ eV}$.⁵² Replacing β - Ga_2O_3 by β - $(\text{In}_x\text{Ga}_{1-x})_2\text{O}_3$ in the channel can further increase $\Delta E_C[\text{channel, barrier}]$ by $\Delta E_C[\beta\text{-}(\text{In}_x\text{Ga}_{1-x})_2\text{O}_3, \beta\text{-Ga}_2\text{O}_3]$

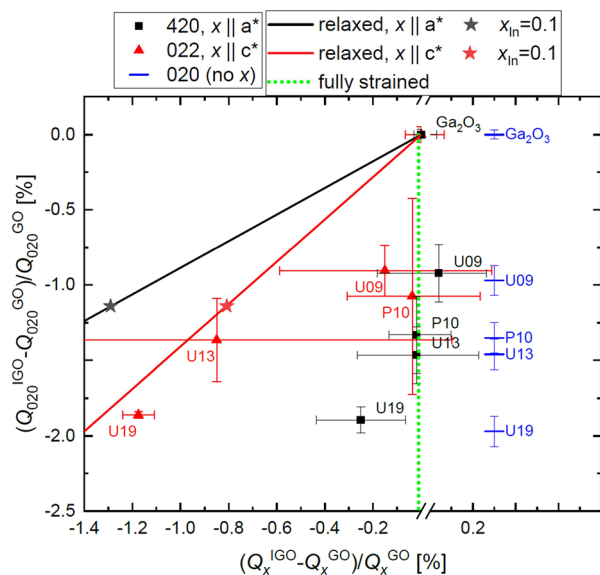


Figure 13. Summary of reciprocal space coordinates of 020, 420, and 022 β -($\text{In}_x\text{Ga}_{1-x}$) $_2\text{O}_3$ reflexes in comparison to those of β - Ga_2O_3 . The error bars reflect the full widths at half maximum values of the reflexes. Expected positions for the relaxed β -($\text{In}_x\text{Ga}_{1-x}$) $_2\text{O}_3$ lattice (from Kranert et al.²⁶) are shown as black and red lines for the 420 and 022 reflexes, respectively.

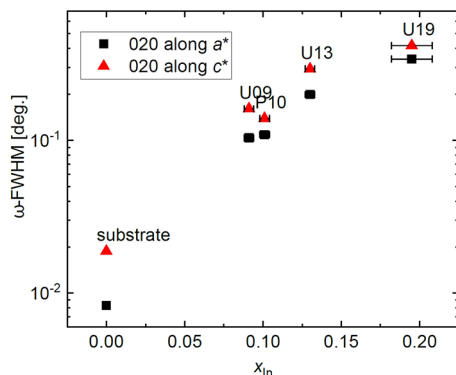


Figure 14. Full widths at half-maximum (FWHM) of the ω -rocking curve of the β -($\text{In}_x\text{Ga}_{1-x}$) $_2\text{O}_3$ 020 reflex along c^* and a^* directions as indicated.

due to the lower lying conduction band of β -($\text{In}_x\text{Ga}_{1-x}$) $_2\text{O}_3$. Theoretical predictions of $\Delta E_C[\beta$ -($\text{In}_x\text{Ga}_{1-x}$) $_2\text{O}_3$, β - Ga_2O_3] are ranging from 1.3 eV for $x = 1$,³³ to 0.4 eV for an epitaxial, (100)-oriented interface with $x = 0.12$.³¹ Assuming the limitation of $x = 0.10$ for a low concentration of extended defects, coherently grown β -($\text{In}_x\text{Ga}_{1-x}$) $_2\text{O}_3$ determined here, $\Delta E_C[\beta$ -($\text{In}_x\text{Ga}_{1-x}$) $_2\text{O}_3$, β - Ga_2O_3] would be limited to 0.13 or 0.33 eV. Thus, $\Delta E_C[\beta$ -($\text{In}_{0.1}\text{Ga}_{0.9}$) $_2\text{O}_3$, β -($\text{Al}_{0.17}\text{Ga}_{0.83}$) $_2\text{O}_3$] would be limited to 0.53 or 0.73 eV, with the prospect to confine a n_s of up to 6.2×10^{12} or $8.6 \times 10^{12} \text{ cm}^{-2}$ instead of $4.7 \times 10^{12} \text{ cm}^{-2}$ for the case of a β - Ga_2O_3 channel. We believe these values to be a lower bound estimate since to confine the 2DEG, β -($\text{In}_{0.1}\text{Ga}_{0.9}$) $_2\text{O}_3$ can be significantly thinner (few nm) than the ~ 120 nm-thick layer (P10) investigated here, thus allowing for potentially higher In-content while maintaining coherent growth as well as providing a back-barrier to the underlying β - Ga_2O_3 . Nevertheless, it should be considered that the increase of n_s may come at the expense of reduced channel mobility due to additional alloy scattering and reduced

breakdown voltage because of the lower bandgap of β -($\text{In}_{0.1}\text{Ga}_{0.9}$) $_2\text{O}_3$ compared to β - Ga_2O_3 .

4. SUMMARY AND CONCLUSIONS

In this work, the growth and structural properties of monoclinic β -($\text{In}_x\text{Ga}_{1-x}$) $_2\text{O}_3$ layers were explored to predict their prospects for the increase of sheet electron concentration n_s of 2DEGs confined in β -($\text{In}_x\text{Ga}_{1-x}$) $_2\text{O}_3$ /($\text{Al}_y\text{Ga}_{1-y}$) $_2\text{O}_3$ heterostructures compared to state-of-the-art β - Ga_2O_3 / β -($\text{Al}_y\text{Ga}_{1-y}$) $_2\text{O}_3$ ones.

For this purpose, 60–180 nm-thick β -($\text{In}_x\text{Ga}_{1-x}$) $_2\text{O}_3$ layers were grown by molecular beam epitaxy on β - Ga_2O_3 substrates in one of the most technologically relevant growth orientations of the monoclinic gallium oxide material system, i.e., (010). With qualitative agreement of the results from two different MBE systems, the collected data give practical experimental guidelines for the control of In content x by growth parameters and demonstrate the possibility of depositing high-quality β -($\text{In}_x\text{Ga}_{1-x}$) $_2\text{O}_3$ layers free from secondary phases or orientations up to at least $x = 0.1$. With such an In content, the conduction band offset confining the 2DEG in β -($\text{In}_x\text{Ga}_{1-x}$) $_2\text{O}_3$ /($\text{Al}_y\text{Ga}_{1-y}$) $_2\text{O}_3$ heterostructures could be at least 0.13 eV larger than in β - Ga_2O_3 /($\text{Al}_y\text{Ga}_{1-y}$) $_2\text{O}_3$ ones, with the prospect to potentially increase n_s from $4.7 \times 10^{12} \text{ cm}^{-2}$ for an Al content of $y = 0.17$ (ref S2) to $> 6.2 \times 10^{12} \text{ cm}^{-2}$.

The strain relaxation with respect to the underlying (010) β - Ga_2O_3 substrate was found to be markedly anisotropic, with faster relaxation into the c^* direction than in the a^* direction. The associated anisotropic dislocation formation could lead to anisotropic in-plane transport in electronic devices with β -($\text{In}_x\text{Ga}_{1-x}$) $_2\text{O}_3$ channels as thick as our layers.

A 2DEG can be contained in significantly thinner β -($\text{In}_x\text{Ga}_{1-x}$) $_2\text{O}_3$ layers than those studied here. Therefore, it is reasonable to assume that their reduced thickness allows for an increased In content, and thus stronger confinement of a higher n_s , without reduction of structural quality.

AUTHOR INFORMATION

Corresponding Author

Piero Mazzolini – Paul-Drude-Institut für Festkörperelektronik, Leibniz-Institut im Forschungsverbund Berlin e.V., 10117 Berlin, Germany; Present Address: Department of Mathematical Physical and Computer Sciences, University of Parma, Parco Area delle Scienze 7/A, 43124 Parma, Italy; orcid.org/0000-0003-2092-5265; Email: piero.mazzolini@unipr.it

Authors

Charlotte Wouters – Leibniz-Institut für Kristallzüchtung, 12489 Berlin, Germany
Martin Albrecht – Leibniz-Institut für Kristallzüchtung, 12489 Berlin, Germany
Andreas Falkenstein – Institute of Physical Chemistry, RWTH Aachen University, D-52056 Aachen, Germany
Manfred Martin – Institute of Physical Chemistry, RWTH Aachen University, D-52056 Aachen, Germany; orcid.org/0000-0001-9046-050X
Patrick Vogt – Materials Department, University of California Santa Barbara, Santa Barbara, California 93106, United States; Present Address: Institute of Solid State Physics, University of Bremen, Otto-Hahn-Allee 1, 28359 Bremen, Germany

Oliver Bierwagen – Paul-Drude-Institut für Festkörperelektronik, Leibniz-Institut im Forschungsverbund Berlin e.V., 10117 Berlin, Germany; orcid.org/0000-0002-4746-5660

Complete contact information is available at: <https://pubs.acs.org/10.1021/acsami.3c19095>

Notes

The authors declare no competing financial interest.

ACKNOWLEDGMENTS

We would like to thank A. Mauze for experimental contributions and J. S. Speck for scientific discussion. We also thank D. V. Dinh and S. Bin Anooz for critically reading the manuscript, as well as Hans-Peter Schönherr, Claudia Herrmann, and Carsten Stemmler for their technical support on the MBE system at PDI. This work was performed in the framework of GraFOx, a Leibniz-ScienceCampus partially funded by the Leibniz association.

REFERENCES

- (1) Pearton, S. J.; Yang, J.; Cary, P. H.; Ren, F.; Kim, J.; Tadjer, M. J.; Mastro, M. A. A review of Ga₂O₃ materials, processing, and devices. *Appl. Phys. Rev.* **2018**, *5* (1), No. 011301.
- (2) Higashiwaki, M.; Sasaki, K.; Kuramata, A.; Masui, T.; Yamakoshi, S. Gallium oxide (Ga₂O₃) metal-semiconductor field-effect transistors on single-crystal β -Ga₂O₃ (010) substrates. *Appl. Phys. Lett.* **2012**, *100* (1), No. 013504.
- (3) Green, A. J.; Speck, J.; Xing, G.; Moens, P.; Allerstam, F.; Gumaelius, K.; Neyer, T.; Arias-Purdue, A.; Mehrotra, V.; Kuramata, A.; Sasaki, K.; Watanabe, S.; Koshi, K.; Blevins, J.; Bierwagen, O.; Krishnamoorthy, S.; Leedy, K.; Arehart, A. R.; Neal, A. T.; Mou, S.; Ringel, S. A.; Kumar, A.; Sharma, A.; Ghosh, K.; Singiseti, U.; Li, W.; Chabak, K.; Liddy, K.; Islam, A.; Rajan, S.; Graham, S.; Choi, S.; Cheng, Z.; Higashiwaki, M. β -Gallium oxide power electronics. *APL Mater.* **2022**, *10* (2), No. 029201.
- (4) Orita, M.; Ohta, H.; Hirano, M.; Hosono, H. Deep-ultraviolet transparent conductive β -Ga₂O₃ thin films. *Appl. Phys. Lett.* **2000**, *77* (25), 4166–4168.
- (5) Tippins, H. H. Optical Absorption and Photoconductivity in the Band Edge of β -Ga₂O₃. *Phys. Rev.* **1965**, *140* (1A), A316–A319.
- (6) Ueda, N.; Hosono, H.; Waseda, R.; Kawazoe, H. Synthesis and control of conductivity of ultraviolet transmitting β -Ga₂O₃ single crystals. *Appl. Phys. Lett.* **1997**, *70* (26), 3561–3563.
- (7) Galazka, Z.; Uecker, R.; Irmscher, K.; Albrecht, M.; Klimm, D.; Pietsch, M.; Brützm, M.; Bertram, R.; Ganschow, S.; Fornari, R. Czochralski growth and characterization of β -Ga₂O₃ single crystals. *Cryst. Res. Technol.* **2010**, *45* (12), 1229–1236.
- (8) Kuramata, Akito; Koshi, Kimiyoshi; Watanabe, Shinya; Yamaoka, Yu; Masui, Takekazu; Yamakoshi, Shigenobu High-quality β -Ga₂O₃ single crystals grown by edge-defined film-fed growth. *Jpn. J. Appl. Phys.* **2016**, *55* (12), 1202A2.
- (9) Fujita, S.; Kaneko, K. Epitaxial growth of corundum-structured wide band gap III-oxide semiconductor thin films. *J. Cryst. Growth* **2014**, *401*, 588–592.
- (10) Zhang, Y.; Neal, A.; Xia, Z.; Joishi, C.; Johnson, J. M.; Zheng, Y.; Bajaj, S.; Brenner, M.; Dorsey, D.; Chabak, K.; Jessen, G.; Hwang, J.; Mou, S.; Heremans, J. P.; Rajan, S. Demonstration of high mobility and quantum transport in modulation-doped β -(Al_xGa_{1-x})₂O₃/Ga₂O₃ heterostructures. *Appl. Phys. Lett.* **2018**, *112* (17), 173502.
- (11) Zhang, Y.; Joishi, C.; Xia, Z.; Brenner, M.; Lodha, S.; Rajan, S. Demonstration of β -(Al_xGa_{1-x})₂O₃/Ga₂O₃ double heterostructure field effect transistors. *Appl. Phys. Lett.* **2018**, *112* (23), 233503.
- (12) Ahmadi, Elaheh; Koksaldi, Onur S.; Zheng, Xun; Mates, Tom; Oshima, Yuichi; Mishra, Umesh K.; Speck, James S. Demonstration of β -(Al_xGa_{1-x})₂O₃/ β -Ga₂O₃ modulation doped field-effect transistors with Ge as dopant grown via plasma-assisted molecular beam epitaxy. *Appl. Phys. Express* **2017**, *10* (7), No. 071101.
- (13) Ranga, P.; Bhattacharyya, A.; Rishinaramangalam, A.; Ooi, Y. K.; Scarpulla, M. A.; Feezell, D. F.; Krishnamoorthy, S. Delta-doped β -Ga₂O₃ thin films and β -(Al_{0.26}Ga_{0.74})₂O₃/ β -Ga₂O₃ heterostructures grown by metalorganic vapor-phase epitaxy. *Appl. Phys. Express* **2020**, *13*, No. 045501.
- (14) Mazzolini, P.; Vogt, P.; Schewski, R.; Wouters, C.; Albrecht, M.; Bierwagen, O. Faceting and metal-exchange catalysis in (010) β -Ga₂O₃ thin films homoepitaxially grown by plasma-assisted molecular beam epitaxy. *APL Mater.* **2019**, *7* (2), No. 022511.
- (15) Sasaki, K.; Kuramata, A.; Masui, T.; Villora, E. G.; Shimamura, K.; Yamakoshi, S. Device-Quality β -Ga₂O₃ Epitaxial Films Fabricated by Ozone Molecular Beam Epitaxy. *Appl. Phys. Express* **2012**, *5* (3), No. 035502.
- (16) Okumura, H.; Kita, M.; Sasaki, K.; Kuramata, A.; Higashiwaki, M.; Speck, J. S. Systematic investigation of the growth rate of β -Ga₂O₃ (010) by plasma-assisted molecular beam epitaxy. *Appl. Phys. Express* **2014**, *7* (9), No. 095501.
- (17) Mazzolini, P.; Falkenstein, A.; Wouters, C.; Schewski, R.; Markurt, T.; Galazka, Z.; Martin, M.; Albrecht, M.; Bierwagen, O. Substrate-Orientation Dependence of β -Ga₂O₃ (100), (010), (001), and (−201) Homoepitaxy by Indium-Mediated Metal-Exchange Catalyzed Molecular Beam Epitaxy (MEXCAT-MBE). *APL Mater.* **2020**, *8*, No. 011107.
- (18) Schewski, R.; Lion, K.; Fiedler, A.; Wouters, C.; Popp, A.; Levchenko, S. V.; Schulz, T.; Schmidbauer, M.; Bin Anooz, S.; Grüneberg, R.; Galazka, Z.; Wagner, G.; Irmscher, K.; Scheffler, M.; Draxl, C.; Albrecht, M. Step-flow growth in homoepitaxy of β -Ga₂O₃ (100)—The influence of the miscut direction and faceting. *APL Mater.* **2019**, *7* (2), No. 022515.
- (19) Mazzolini, P.; Bierwagen, O. Towards smooth (010) β -Ga₂O₃ films homoepitaxially grown by plasma assisted molecular beam epitaxy: the impact of substrate offset and metal-to-oxygen flux ratio. *J. Phys. Appl. Phys.* **2020**, *53* (35), 354003.
- (20) Mazzolini, P.; Falkenstein, A.; Galazka, Z.; Martin, M.; Bierwagen, O. Offcut-related step-flow and growth rate enhancement during (100) β -Ga₂O₃ homoepitaxy by metal-exchange catalyzed molecular beam epitaxy (MEXCAT-MBE). *Appl. Phys. Lett.* **2020**, *117* (22), 222105.
- (21) Vogt, P.; Mauze, A.; Wu, F.; Bonef, B.; Speck, J. S. Metal-oxide catalyzed epitaxy (MOCATAXY): the example of the O plasma-assisted molecular beam epitaxy of β -(Al_xGa_{1-x})₂O₃/ β -Ga₂O₃ heterostructures. *Appl. Phys. Express* **2018**, *11* (11), No. 115503.
- (22) Bin Anooz, S.; Popp, A.; Grüneberg, R.; Wouters, C.; Schewski, R.; Schmidbauer, M.; Albrecht, M.; Fiedler, A.; Ramsteiner, M.; Klimm, D.; Irmscher, K.; Galazka, Z.; Wagner, G. Indium incorporation in homoepitaxial β -Ga₂O₃ thin films grown by metal organic vapor phase epitaxy. *J. Appl. Phys.* **2019**, *125* (19), 195702.
- (23) Bin Anooz, S.; Grüneberg, R.; Wouters, C.; Schewski, R.; Albrecht, M.; Fiedler, A.; Irmscher, K.; Galazka, Z.; Miller, W.; Wagner, G.; Schwarzkopf, J.; Popp, A. Step flow growth of β -Ga₂O₃ thin films on vicinal (100) β -Ga₂O₃ substrates grown by MOVPE. *Appl. Phys. Lett.* **2020**, *116* (18), 182106.
- (24) Mauze, A.; Zhang, Y.; Itoh, T.; Wu, F.; Speck, J. S. Metal oxide catalyzed epitaxy (MOCATAXY) of β -Ga₂O₃ films in various orientations grown by plasma-assisted molecular beam epitaxy. *APL Mater.* **2020**, *8* (2), No. 021104.
- (25) Baldini, M.; Gogova, D.; Irmscher, K.; Schmidbauer, M.; Wagner, G.; Fornari, R. Heteroepitaxy of Ga₂(1-x)In_{2x}O₃ layers by MOVPE with two different oxygen sources. *Cryst. Res. Technol.* **2014**, *49* (8), 552–557.
- (26) Kranert, C.; Lenzner, J.; Jenderka, M.; Lorenz, M.; von Wenckstern, H.; Schmidt-Grund, R.; Grundmann, M. Lattice parameters and Raman-active phonon modes of (In_xGa_{1-x})₂O₃ for $x < 0.4$. *J. Appl. Phys.* **2014**, *116* (1), No. 013505.
- (27) Oshima, T.; Fujita, S. Properties of Ga₂O₃-based (In_xGa_{1-x})₂O₃ alloy thin films grown by molecular beam epitaxy. *Phys. Status Solidi C* **2008**, *5* (9), 3113–3115.

- (28) Vogt, P.; Bierwagen, O. Kinetics versus thermodynamics of the metal incorporation in molecular beam epitaxy of $(\text{In}_x\text{Ga}_{1-x})_2\text{O}_3$. *APL Mater.* **2016**, *4* (8), No. 086112.
- (29) Rafique, S.; Han, L.; Neal, A. T.; Mou, S.; Boeckl, J.; Zhao, H. Towards High-Mobility Heteroepitaxial β -Ga₂O₃ on Sapphire – Dependence on The Substrate Off-Axis Angle. *Phys. Status Solidi A* **2018**, *215* (2), 1700467.
- (30) Baldini, M.; Albrecht, M.; Gogova, D.; Schewski, R.; Wagner, G. Effect of indium as a surfactant in $(\text{Ga}_{1-x}\text{In}_x)_2\text{O}_3$ epitaxial growth on β -Ga₂O₃ by metal organic vapour phase epitaxy. *Semicond. Sci. Technol.* **2015**, *30* (2), No. 024013.
- (31) Maccioni, M. B.; Ricci, F.; Fiorentini, V. Low In solubility and band offsets in the small-x β -Ga₂O₃/ $(\text{Ga}_{1-x}\text{In}_x)_2\text{O}_3$ system. *Appl. Phys. Express* **2015**, *8* (2), No. 021102.
- (32) Maccioni, M. B.; Fiorentini, V. Phase diagram and polarization of stable phases of $(\text{Ga}_{1-x}\text{In}_x)_2\text{O}_3$. *Appl. Phys. Express* **2016**, *9* (4), No. 041102.
- (33) Peelaers, H.; Steiauf, D.; Varley, J. B.; Janotti, A.; Van de Walle, C. G. $(\text{In}_x\text{Ga}_{1-x})_2\text{O}_3$ alloys for transparent electronics. *Phys. Rev. B* **2015**, *92* (8), No. 085206.
- (34) Edwards, D. D.; Folkins, P. E.; Mason, T. O. Phase Equilibria in the Ga₂O₃ In₂O₃ System. *J. Am. Ceram. Soc.* **1997**, *80* (1), 253–257.
- (35) von Wenckstern, H.; Splith, D.; Werner, A.; Müller, S.; Lorenz, M.; Grundmann, M. Properties of Schottky Barrier Diodes on $(\text{In}_x\text{Ga}_{1-x})_2\text{O}_3$ for $0.01 \leq x \leq 0.85$ Determined by a Combinatorial Approach. *ACS Comb. Sci.* **2015**, *17* (12), 710–715.
- (36) Boschi, F.; Bosi, M.; Berzina, T.; Buffagni, E.; Ferrari, C.; Fornari, R. Hetero-epitaxy of ϵ -Ga₂O₃ layers by MOCVD and ALD. *J. Cryst. Growth* **2016**, *443*, 25–30.
- (37) Cora, I.; Mezzadri, F.; Boschi, F.; Bosi, M.; Čaplovičová, M.; Calestani, G.; Dódony, I.; Pécz, B.; Fornari, R. The real structure of ϵ -Ga₂O₃ and its relation to κ -phase. *CrystEngComm* **2017**, *19* (11), 1509–1516.
- (38) Vogt, P.; Brandt, O.; Riechert, H.; Lähnemann, J.; Bierwagen, O. Metal-Exchange Catalysis in the Growth of Sesquioxides: Towards Heterostructures of Transparent Oxide Semiconductors. *Phys. Rev. Lett.* **2017**, *119* (19), No. 196001.
- (39) Kracht, M.; Karg, A.; Schörmann, J.; Weinhold, M.; Zink, D.; Michel, F.; Rohnke, M.; Schowalter, M.; Gerken, B.; Rosenauer, A.; Klar, P. J.; Janek, J.; Eickhoff, M. Tin-Assisted Synthesis of ϵ -Ga₂O₃ by Molecular Beam Epitaxy. *Phys. Rev. Appl.* **2017**, *8* (5), No. 054002.
- (40) Bierwagen, O.; Vogt, P.; Mazzolini, P., In *Gallium Oxide: Materials Properties, Crystal Growth, and Devices*; Higashiwaki, M.; Fujita, S. (Eds.). Springer International Publishing: Cham, 2020, pp. 95–121, DOI: 10.1007/978-3-030-37153-1_6.
- (41) Vogt, P.; Hensling, F. V. E.; Azizie, K.; McCandless, J. P.; Park, J.; DeLello, K.; Muller, D. A.; Xing, H. G.; Jena, D.; Schlom, D. G. Extending the Kinetic and Thermodynamic Limits of Molecular-Beam Epitaxy Utilizing Suboxide Sources or Metal-Oxide-Catalyzed Epitaxy. *Phys. Rev. Appl.* **2022**, *17* (3), No. 034021.
- (42) McCandless, J. P.; Rowe, D.; Pieczulewski, N.; Protasenko, V.; Alonso-Orts, M.; Williams, M. S.; Eickhoff, M.; Xing, H. G.; Muller, D. A.; Jena, D.; Vogt, P. Growth of α -Ga₂O₃ on α -Al₂O₃ by conventional molecular-beam epitaxy and metal-oxide-catalyzed epitaxy. *Jpn. J. Appl. Phys.* **2023**, *62*, SF1013.
- (43) Karg, A.; Kracht, M.; Vogt, P.; Messow, A.; Braud, N.; Schörmann, J.; Rohnke, M.; Janek, J.; Falta, J.; Eickhoff, M. Enhanced epitaxial growth of Ga₂O₃ using an ultrathin SnO₂ layer. *J. Appl. Phys.* **2022**, *132* (19), 195304.
- (44) Ardenghi, A.; Bierwagen, O.; Lähnemann, J.; Kler, J.; Falkenstein, A.; Martin, M.; Mazzolini, P. Phase-selective growth of κ - vs β -Ga₂O₃ and $(\text{In}_x\text{Ga}_{1-x})_2\text{O}_3$ by In-mediated metal exchange catalysis in plasma-assisted molecular beam epitaxy. 2023, arXiv:2311.13318. arXiv.org e-Print archive. <https://arxiv.org/abs/2311.13318>.
- (45) Karg, A.; Hinz, A.; Figge, S.; Schowalter, M.; Vogt, P.; Rosenauer, A.; Eickhoff, M. Indium: A surfactant for the growth of ϵ/κ -Ga₂O₃ by molecular beam epitaxy. *APL Mater.* **2023**, *11* (9), No. 091114.
- (46) Williams, M.S.; Alonso-Orts, M.; Schowalter, M.; Karg, A.; Raghuvansy, S.; McCandless, J.P.; Jena, D.; Rosenauer, A.; Eickhoff, M.; Vogt, P. *Growth, catalysis and faceting of α -Ga₂O₃ and α - $(\text{In}_x\text{Ga}_{1-x})_2\text{O}_3$ on m -plane α -Al₂O₃ by molecular beam epitaxy*, 2023. <https://arxiv.org/abs/2311.12460>.
- (47) Oshima, Y.; Ahmadi, E.; Badescu, S. C.; Wu, F.; Speck, J. S. Composition determination of beta- $(\text{Al}_x\text{Ga}_{1-x})_2\text{O}_3$ layers coherently grown on (010) beta-Ga₂O₃ substrates by high-resolution X-ray diffraction. *Appl. Phys. Express* **2016**, *9* (6), No. 061102.
- (48) Cheng, Z.; Hanke, M.; Vogt, P.; Bierwagen, O.; Trampert, A. Phase formation and strain relaxation of Ga₂O₃ on c -plane and a -plane sapphire substrates as studied by synchrotron-based x-ray diffraction. *Appl. Phys. Lett.* **2017**, *111* (16), 162104.
- (49) Reis, A.; Hanke, M.; Lopes, J. M. J.; Trampert, A. Anisotropic strain relaxation in epitaxially constrained α - $(\text{Al},\text{Ga})_2\text{O}_3$ thin films on a -plane Al₂O₃. *Appl. Phys. Lett.* **2023**, *123* (12), 122102.
- (50) Luan, S.; Dong, L.; Jia, R. Analysis of the structural, anisotropic elastic and electronic properties of β -Ga₂O₃ with various pressures. *J. Cryst. Growth* **2019**, *505*, 74–81.
- (51) Golz, C.; Galazka, Z.; Lähnemann, J.; Hortelano, V.; Hatami, F.; Masselink, W. T.; Bierwagen, O. Electrical conductivity tensor of β -Ga₂O₃ analyzed by van der Pauw measurements: Inherent anisotropy, off-diagonal element, and the impact of grain boundaries. *Phys. Rev. Mater.* **2019**, *3* (12), No. 124604.
- (52) Kalarickal, N. K.; Xia, Z.; McGlone, J. F.; Liu, Y.; Moore, W.; Arehart, A. R.; Ringel, S. A.; Rajan, S. High electron density β - $(\text{Al}_{0.17}\text{Ga}_{0.83})_2\text{O}_3/\text{Ga}_2\text{O}_3$ modulation doping using an ultra-thin (1 nm) spacer layer. *J. Appl. Phys.* **2020**, *127* (21), 215706.